I INTRODUCTION

The software DDSURF for a Windows based PC system is a group of codes used to predict electromagnetic scattering from illuminated features present either in free space, on top of a flat surface, or suspended above a flat surface. DDSURF consists of three main executable codes: (1) *createtar07.exe*– which configures the dipole lattice array used to model the geometry of the feature; (2) *ddsurf07.exe* - which calculates the internal field (dipole moment distribution) within the scattering feature; and (3) ffsurf07.exe- which uses the internal field (dipole moment distribution) to determine the external far-field quantities of the scattered field. These quantities include the scattered irradiance and electromagnetic field distribution, and the total scattering cross-section.

DDSURF is based on the *Discrete-Dipole Approximation* method (DDA), also referred to as the coupled-dipole approximation method. The DDA uses the excitation response of electromagnetic dipoles to model the electromagnetic scattering characteristics of a feature. The dipoles are placed in a lattice configuration which models the physical geometries of the scattering feature. CREATETAR creates the lattice configuration used by DDSURF. Using an iterative process to solve the interaction equations of electromagnetically excited dipoles, DDSURF computes the feature internal dipole moment distribution. FFSURF computes the external scattered field by applying the far-field Green's function to the dipole moment distribution found by DDSURF.

In the DDSURF User's Manual, we first discuss the theoretical background of the DDA method used in the development of the codes. Next we discuss the process in which DDSURF was validated, showing comparisons with experiments that were conducted at Arizona State University. Next, we discuss the codes of DDSURF, first how to use the pre-processor CREATETAR to develop the scattering feature dipole lattice configuration. Next, we discuss the DDSURF code itself, what input parameters are needed, and what the steps are needed to run the code. The aspects of the output data files of DDSURF are discussed next. Then the post-processor FFSURF is discussed next, and what parameters will be needed for that code, and what output files can be created with its execution. There are a variety of options to evaluate the results of FFSURF. For example, the scattered irradiance distributions can be plotted, as well as the differential scattering cross-section. Appendix C shows examples of the output files of DDSURF and FFSURF.

II THEORY

II.1 The Discrete-Dipole Approximation Method (Computation of the Internal Field of the Scattering Feature)

Starting from the molecular level, we will discuss the theory behind the discrete-dipole approximation (DDA) method used to model the electromagnetic scattering from features. Molecules are usually electrically neutral, but they are made of atoms which contain positively charge nuclei and negatively charged electrons. When an electric field is present on an atom, the nucleus moves a small distance in the direction of the field while the electrons move in the opposite direction, thus creating an oscillating *dipole*. Figure 2.1 shows an example of a dipole:

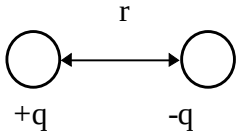

Figure 2.1 Example of an electric dipole.

Similar to the magnetic moment and field created by a magnetic bar with two different poles, the result of separation of the two charges by a distance is a dipole moment and an electric field.

The discrete-dipole approximation method (DDA) was first developed by Purcell and Pennypacker (1973) and later studied by other researchers such as Draine (1988) and Taubenblatt and Tran (1993). In the DDA, sub volumes of features subjected to an electric field are modeled as discrete dipoles. Figure 2.2 shows an example of a dipole configuration for a scattering feature on a surface.

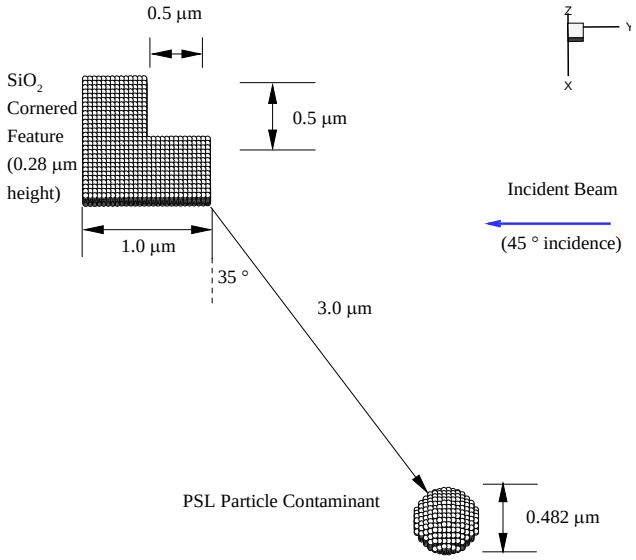

Figure 2.2 Example of dipole configuration for a cornered feature with a spherical particle contaminant on a surface.

The electromagnetic response of each dipole can be determined mathematically by the dipole equations. The dipole moment at the dipole is related to the incident electric field by:

$$\overline{P}_i = \alpha_i \overline{E}_{tot,i} \tag{2-1}$$

$\overline{P}_i$ is the dipole moment at dipole *i*, $\overline{E}_{tot,i}$ is the total electric field at dipole *i*, and α_i is the dipole polarizability. The polarizability is a function of the dipole size and feature material. There has been extensive work to correctly model the polarizability, thus several methods are available. DDSURF uses the lattice dispersion relation (LDR), developed by Draine and Goodman (1993), and has extended this method to model non-spherical dipoles.

The field at a dipole, $\overline{E}_{tot,i}$, can be characterized into several modes. These modes include the direct field from the electrical field incident upon the features and the electric field contribution from the other interacting dipoles. There are two parts to each of these modes, the direct field, and the field when the interacting surface is involved

The electric field can be represented in equation form as:

$$\overline{E}_{tot,i} = \overline{E}_{o,i} + \overline{E}_{direct,i} + \overline{E}_{reflected,i} \tag{2-2}$$

Substituting this into Eq. (2-1), we can make the dipole equation into the form:

$$\left(\alpha_i\right)^{-1} \overline{P}_i - \overline{E}_{direct,i} - \overline{E}_{reflected,i} = \overline{E}_{o,i} \tag{2-3}$$

We will now discuss the three components of the electric field at a dipole.

Electric Field by Incident Beam

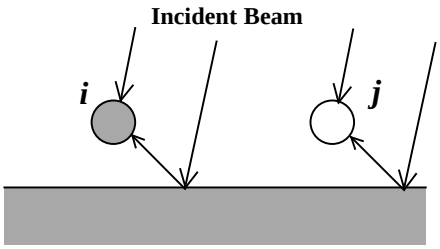

The field due to the light beam incident on the feature has two components, the direct beam, and the field that was reflected from the surface. The reflected field can be computed using the Fresnel reflection equations. Thus the field from the incident beam, $\overline{E}_{o,i}$, has the following form in the *x*, *y*, and *z* components:

$$E_x = E_{0x}\left(e^{-ik_z z} - R^{TM} e^{ik_z z}\right)e^{ik_x x} \tag{2-4a}$$

$$E_y = E_{0y}\left(e^{-ik_z z} + R^{TE} e^{ik_z z}\right)e^{ik_x x} \tag{2-4b}$$

$$E_z = E_{0z}\left(e^{-ik_z z} + R^{TE} e^{ik_z z}\right)e^{ik_x x} \tag{2-4c}$$

The reflection coefficients are described in Appendix B.

Electric Field by Direct Dipole Interaction

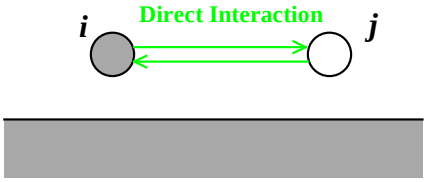

The DDSCAT code developed by Draine and Flatau (1994) considered only direct interaction between dipoles, that is, there was no reflection interaction with a surface. The electric field at a particular dipole, *i*, due to the field emitted by the other dipoles, *j*, in the scattering feature, $\overline{E}_{direct,i}$, can be computed by the summation:

$$\overline{E}_{direct,i} = \frac{k_0^2}{\varepsilon_0}\sum_{j\neq i}\overline{G}_{ij}\cdot\overline{P}_j \tag{2-5}$$

Where k_0 is the wave number in free space, and ε_0 is the permittivity of free space. The Green's function, $\overline{G}_{ij}$ is defined in Appendix B.

Electric Field by Reflected Dipole Interaction

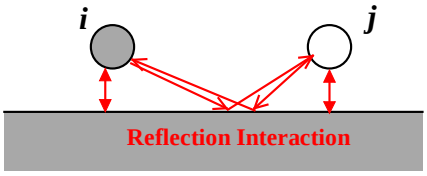

A unique component of DDSURF is the modeling of the dipole radiation that is reflected at the surface. The dipole interaction with the surface occurs in the near-field zone, thus when the electric field interacts with the surface, it does not act as a plane wave. Thus the sole use of Fresnel coefficients to determine the reflected fields is not an accurate model. To deal with the near-field effects, the Sommerfeld integrals are used.

A derivation to determine for the electric field for a dipole above a surface is given by Baños (Baños, 1966). Baños separates the radiating electric field into two components, E_ρ, the electric field in the plane parallel to the surface (*x* and *y* directions), and E_z, the electric field in the plane perpendicular to the surface (*z* direction.)

$$E_\rho(r) = \frac{p}{\varepsilon_1}\left\{\frac{\partial^2}{\partial\rho\partial z}\frac{e^{ik_1 r}}{4\pi r}\right\} \tag{2-6a}$$

$$E_z(r) = \frac{p}{\varepsilon_0}\left\{\left(k_2^2 + \frac{\partial^2}{\partial z^2}\right)\frac{e^{ik_2 r}}{4\pi r}\right\} \tag{2-6b}$$

Through the years, much work has been conducted to evaluate these equations. In particular, the Sommerfeld integral relation states:

$$\frac{e^{ikr}}{r} = i\int_0^\infty \frac{k_\rho}{k_z} J_0\left(k_\rho\rho\right)e^{ik_z|z|}dk_\rho \tag{2-7}$$

There has been extensive investigation on numerical methods to integrate this integral (Lager *et al.*, 1974; Mohsen, 1982). DDSURF uses routines developed by Lytle for evaluating the Sommerfeld integral relation. With the use of these routines, the reflected component of the electric field due to a radiating dipole in the near field can be represented as:

$$\overline{E}_{reflected,i} = \sum_{j=1}^{N}\left(\overline{S}_{ij} + \frac{k_2^2}{\varepsilon_1}\frac{k_1^2 - k_2^2}{k_1^2 + k_2^2}\overline{G}_{ij}^{\,I}\right)\cdot\overline{P}_j\,. \tag{2-8}$$

$\overline{S}_{ij}$ is a 3 x 3 matrix which are Sommerfeld integral expressions, which are determined by the routines provided by Lager (Lager *et al.*, 1974), where k_1 and k_2 are the wave numbers for the particle and the surface respectively, and ε_1 is the permittivity. For the form of $\overline{S}_{ij}$, refer to Schmehl et al. (1997). The image dyadic Green's function is defined as (Schmehl, 1994)

$$\overline{G}_{ij}^{\,I} = -\overline{G}_{ij}\cdot\bar{I}_R, \tag{2-9}$$

where $\bar{I}_R$ is the reflection dyad $\bar{I}_R = \mathbf{e}_x\mathbf{e}_x + \mathbf{e}_y\mathbf{e}_y - \mathbf{e}_z\mathbf{e}_z$. The dyadic product inverts the sign of the first two columns of the matrix of the dyadic Green's function, but leaves the third column unchanged.

Solution of the System of Equations

Now we are able to consider simultaneously all of the dipoles within the lattice. As a result, this will create a matrix equation, which we will denote as the Dipole Matrix Equation. To solve Eq. (2-1) for N dipoles simultaneously, we form the matrix equation:

$$\left(\overline{B} + \overline{A} + \overline{R}\right)\overline{P} = \overline{E}_0\,. \tag{2-10}$$

$\overline{B}$ is a diagonal matrix of the inverse of the dipole polarizabilities. $\overline{A}$ includes the effects of the direct interaction between the dipoles (Eq. (2-3)). $\overline{A}$ involves the dyadic Green's function, and thus distance vectors between each dipole. $\overline{R}$ includes the effect of the reflection interaction between the dipoles and the surface (Eq. 4), which

includes the Sommerfeld integral terms and the image dyadic Green's function, thus also the distance vectors between the dipoles (Schmehl *et al.*, 1997).

Method of Solution

The size of the 3N x 3N non-sparse coefficient matrix $\overline{B} + \overline{A} + \overline{R}$ can be so large such that using a direct matrix inversion method to solve for $\overline{P}$ is impractical. Methods which employ iterative procedures is an alternative to efficiently solve for the system of equation. During the development of DDSURF, several iterative procedures were investigated. Complex conjugate gradient-type (CCG) methods such as the biconjugate gradient (BCG) method and conjugate gradient squared (CGS) method were investigated along with several forms of the Quasi-Minimal Residual (QMR) method. Due to the characteristics of the coefficient matrix, the convergence towards an accurate answer is dependent on scattering feature size and refractive index. The effectiveness of the iterative procedure was based on the ability to converge to an accurate answer in the most reasonable amount of time. DDSURF uses the QMR method developed by Freund (1992). The QMR method follows Algorithm 3.2 in Freund (1992).

The QMR method requires approximately $\boldsymbol{O}(N^2)$ mathematical operations per iteration. When a large number of dipoles are used to model a feature, the computational time would become significantly longer. To reduce the number of operations required, a two-dimensional fast Fourier transform (FFT) is applied to the system of equations (Schmehl, 1994, Nebeker *et al.* 1996). Implementation of the FFT reduces the operations per iteration to $\boldsymbol{O}(\text{NlogN})$, which offers a significant amount of savings in time.

The QMR method iterates towards a solution to the Dipole Matrix Equation (Eq. 9) to a point where the Euclidean norm of the residual was smaller than the convergence criterion.

$$\overline{Z}^{(iter)} = \overline{E}_{inc} - \left(\overline{B} + \overline{A} + \overline{R}\right)\overline{P}^{(iter)} \text{ (residual)} \tag{2-11}$$

$$\frac{\left\|\overline{Z}^{(iter)}\right\|_2}{\left\|\overline{E}_{inc}\right\|_2} \le 10^{-n} \text{ (convergence criterion)} \tag{2-12}$$

$$\left\|\left(\ \right)\right\|_2 = \left(\sum_{i=1}^{3N}\left(\ \right)\cdot\left(\ \right)^*\right)^{1/2} \text{ (Euclidean (2) norm)} \tag{2-13}$$

II.2 Computation of the External Field

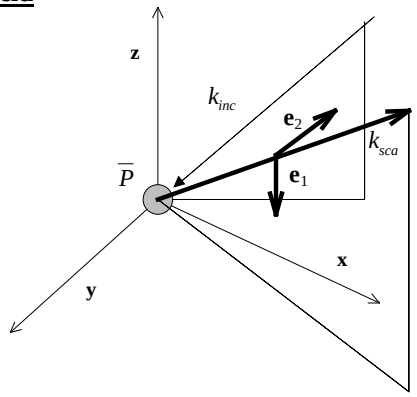

Figure 2.3. Geometrical configuration for far field scattering.

Once DDSURF has reached convergence, the user can execute FFSURF to calculate the far field electric field, the irradiance, the total scattering cross-section, and the differential scattering cross-section. From the particle to the receiving detector, there are two scattering components to consider. One component is the field radiated directly

from the dipole without interaction with a surface. Assuming that $r >> r_j$, and in terms of the scattering frame of reference as shown in Fig. 2.3, this is:

$$\overline{E}_{direct,i} = \frac{k_0^2}{\varepsilon_0} \sum_{j \neq i} \overline{G}_{ij} \cdot \overline{P}_j \tag{2-14a}$$

If we were to consider this in terms of the scattering reference frame, this reduces to:

$$\overline{E}_{sca,direct}(r) = k_0^2 \frac{\exp(ik_0 r)}{4\pi r} \sum_{j=1}^{N} \left\{ \exp(-i\,\mathrm{k}_{sca} \cdot \mathrm{r}_j) \left[\left(\overline{P}_j \cdot \mathrm{e}_1 \right) \mathrm{e}_1 + \left(\overline{P}_j \cdot \mathrm{e}_2 \right) \mathrm{e}_2 \right] \right\} \tag{2-14b}$$

by direct scattering from each dipole.

The second component of the field that is present at the detection region is the field that is radiated from the dipole, but also reflects off of the surface. In the scattering far-field, the Fresnel scattering coefficients can be used to account for the interaction with the surface. We can use Eq. (2-14b) to determine the reflected component of the direct field . To determine the reflected field component, the method of images altered with the Fresnel coefficients to account for the dielectric surface:

$$\overline{E}_{sca,refl}(r) = k_0^2 \frac{\exp(ik_0 r)}{4\pi r} \sum_{j=1}^{N} \left\{ \exp(-i\,\mathrm{k}_{sca}^{I} \cdot \mathrm{r}_{I,j}) \left[R^{TM} \left(\overline{P}_j \cdot \mathrm{e}_1 \right) \mathrm{e}_1 + R^{TE} \left(\overline{P}_j \cdot \mathrm{e}_2 \right) \mathrm{e}_2 \right] \right\}, \tag{2-15}$$

where R^{TM} and R^{TE} are the Fresnel reflection coefficients which are defined in Appendix B.

Summing Eqs. (2-14b) and (2-15) we get:

$$\overline{E}_{sca}(r) = k_0^2 \frac{\exp(ik_0 r)}{4\pi r} \sum_{j=1}^{N} \left\{ \begin{array}{l} \exp(-ik_{sca} r_j) \left[\left(\overline{P}_j \cdot \mathrm{e}_1 \right) \mathrm{e}_1 + \left(\overline{P}_j \cdot \mathrm{e}_2 \right) \mathrm{e}_2 \right] + \\ \exp(-ik_{sca} r_j) \left[R^{TM} \left(\overline{P}_j \cdot \mathrm{e}_1 \right) \mathrm{e}_1 + R^{TE} \left(\overline{P}_j \cdot \mathrm{e}_2 \right) \mathrm{e}_2 \right] \end{array} \right\}. \tag{2-16}$$

The far-field irradiance can be found by multiplying the scattered electric field by its complex conjugate:

$$I_{sca}(r) = \overline{E}_{sca}(r) \overline{E}_{sca}^{\Psi}(r). \tag{2-17}$$

Once the irradiance is found, the total scattering cross-section, C_{sca}, and the differential scattering cross-section, $dC_{sc} / d\Omega$, can be determined.

The total scattering cross section, C_{sca} is defined as (Bawolek, 1991):

$$C_{sca} = \frac{P_{sca}}{I_0} \tag{2-18}$$

where P_{sca} is the power collected by some detector, and I_0 is the incident irradiance at the center of the Gaussian beam.

The differential scattering cross-section is defined as the energy scattered per unit time into a unit solid angle about a certain direction. Bohren and Huffman[11] derived an expression for this:

$$\frac{dC_{sca}}{d\Omega} = \lim_{\Omega \to 0} \left(\frac{C_{sca}}{\Omega} \right) \approx \frac{I_{sca} A}{I_0 \left(A / r^2 \right)} = \frac{r^2 I_{sca}}{I_0}, \tag{2-19}$$

where I_{sca} is the scattered irradiance, A is the detection area scattered to, r is the distance from the particle to the observation point, and Ω is the solid angle.

III. COMPARISON WITH EXPERIMENT

Experiments were conducted at Arizona State University by Greg Starr to determine the validity and accuracy of DDSURF and FFSURF. Light scattering measurements from a number of feature configurations were conducted using a scatterometer and the ring/wedge detector shown in Figure 3.1.

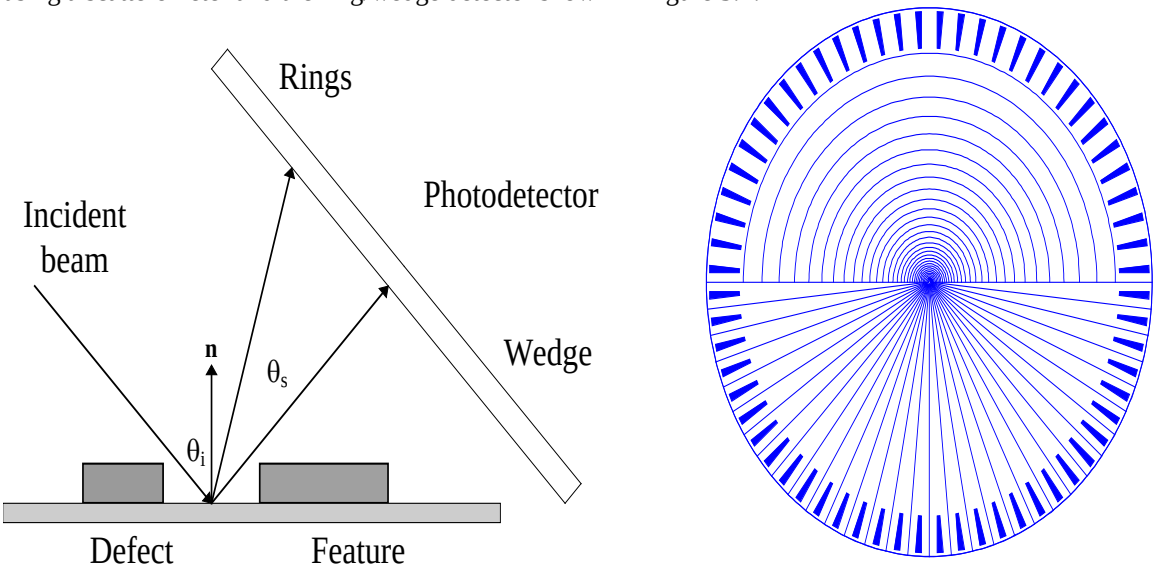

Figure 3.1 (a) Side view of beam, substrate and photodetector configuration; (b) photodetector ring/wedge configuration

The ASU scatterometer can use a helium-neon laser beam (λ = 632.8 nm), or an argon-ion laser beam (λ = 488 nm) to create the scattering signature from the feature on a surface. The ring/wedge photodetector which consists of 32 rings and 32 wedges that act as individual detectors detect the scattered light from the feature on the surface. The detector is centered on the specular, and the incident angle (θ_I) has been studied at 45 deg and 70 deg from the surface normal, and the distance from the feature to the detector center is approximately 8.2 mm.

III.1 Complex Shapes on Surface

DDSURF has been used to model light scattering from SiO_2 patterned features present within the Arizona State University/Semiconductor Research Corporation block of the SEMATECH patterned wafer defect standard die. PSL spheres were deposited on the patterned wafer to act as particle contamination. An overhead view of the SEM photograph and the dipole configuration of the SiO_2 cornered feature with a PSL sphere contaminant are shown in Figures 3.2.

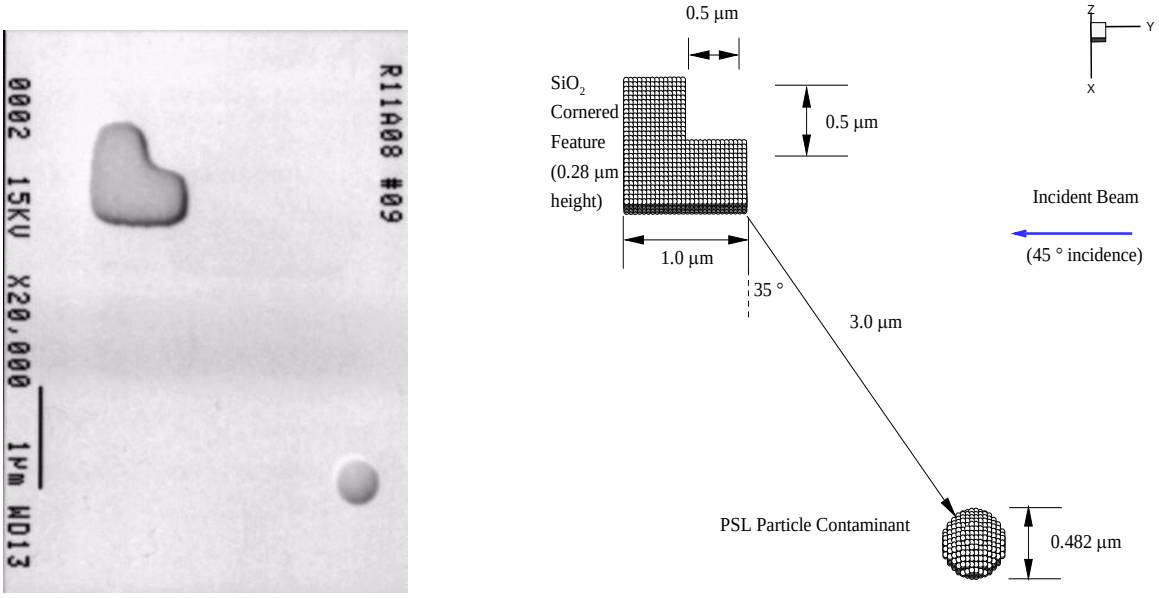

(a) (b)

Figure 3.2 (a) SEM photo of a SiO2 cornered feature with a PSL particle contaminant; (b) dipole configuration used for the DDSURF modeling of the features.

Figure 3.3a shows the computed irradiance distribution for scattering from the SiO_2 corner only, at the region where the detector occupied during the experiment. Figure 3.3b shows the irradiance distribution of the scattering when the particle contaminant is introduced.

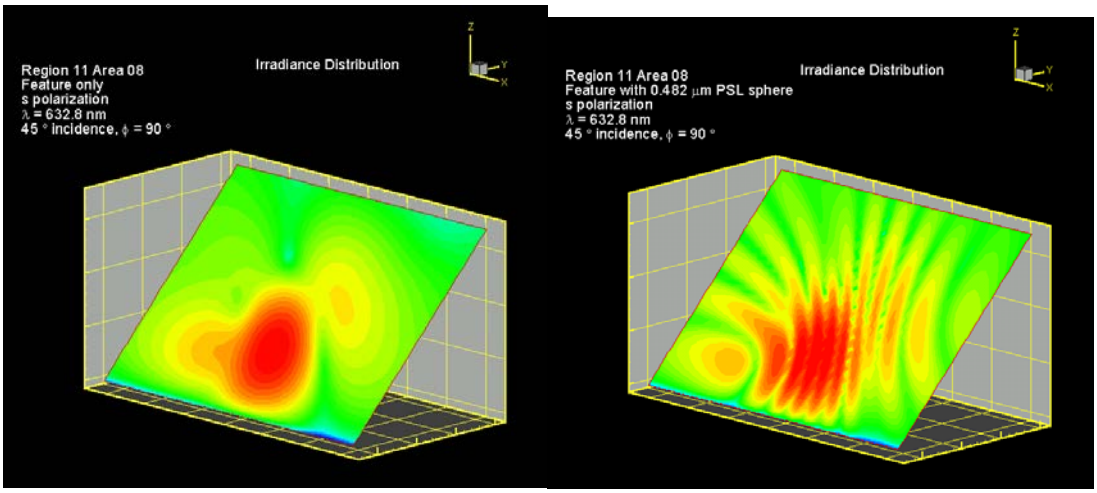

(a) (b)

Figure 3.3 Irradiance distribution on detector plane for SiO_2 cornered feature: (a) feature only, (b) feature with contaminating 0.482 µm PSL sphere on a silicon surface.

Figures 3.4(a)-(b) and Figures 3.5(a)-(b) show the quantitative comparisons of the differential scattering cross-sections found by experiments conducted at Arizona State University and the results from DDSURF. We see that the comparisons are very close to each other.

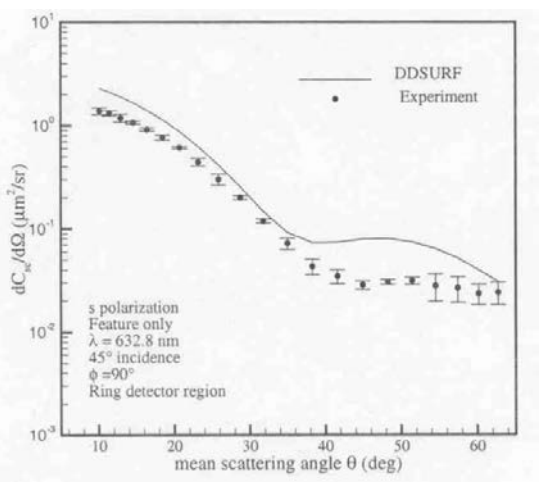

(a)

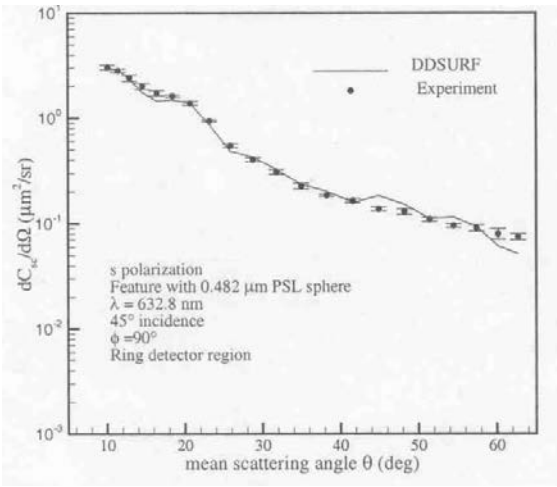

(b)

Figure 3.4 (a) $dC_{sca}/d\Omega$ angular variation in ring region for SiO_2 cornered feature: (a) feature only, (b) feature with 0.482 μm PSL contaminant sphere on a silicon surface.

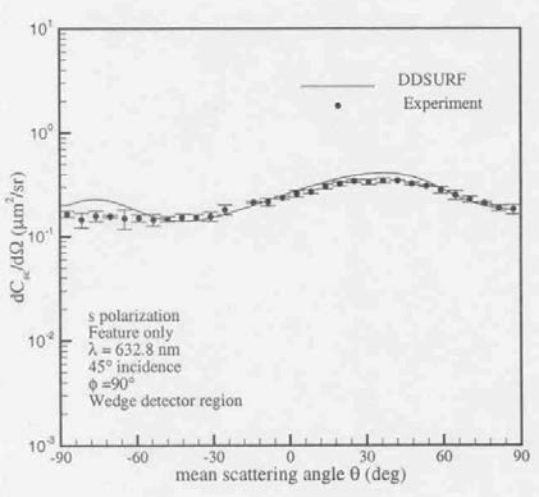

(a)

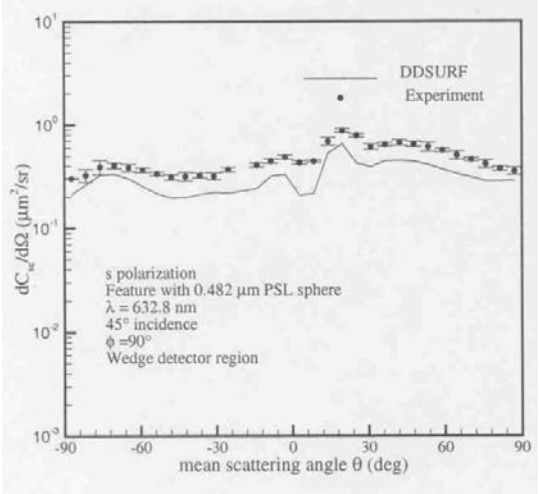

(b)

Figure 3.5 (a) $dC_{sca}/d\Omega$ angular variation in wedge region for SiO_2 cornered feature: (a) feature only, (b) feature with 0.482 μm PSL contaminant sphere on a silicon surface.

III.2 Features on Filmed Surfaces

To study the accuracy of the filmed-based DDSURF, which is also referred to as DDFILM, experiments were conducted at Arizona State University for spherical particles which were placed on a filmed substrate. The scattered field was measured using the laser scatterometer at the Laser Diagnostics laboratory. Figures 3.6(a) and 3.6(b) show the p and s polarization cases respectively for scattering from a 0.305 μm PSL sphere which lies upon a silicon substrate with a 0.25 μm SiO_2 film. The detection region used was that for the ring section of the ring/wedge detection system shown in Fig. 3.1. The incident beam was at 70 degrees from the surface normal. The comparisons are good and the DDFILM results lie within the uncertainty levels of the experiment.

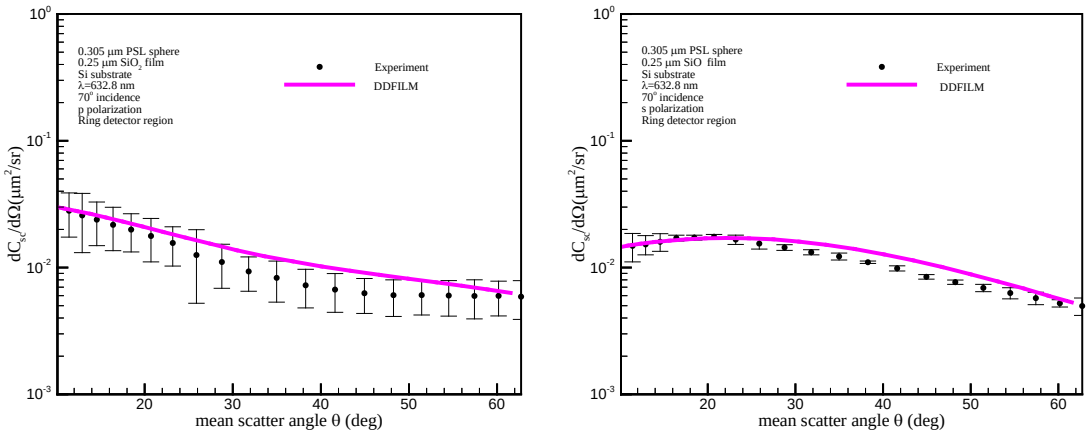

Figure 3.6 $dC_{sca}/d\Omega$ angular variation in ring region for a 0.305 μm PSL sphere on a Si substrate with a 0.25 μm SiO_2 film. Incident beam is at 70 deg incidence, 632.8 nm wavelength, and: (a) p polarization, (b) s polarization.

Figure 3.7 shows comparisons of the differential scattering cross-section found using the Filmed DDSURF (DDFILM) and experiment conducted at Arizona State University using a point silicon detector. The scattering angle is the theta distribution along the plane of incidence. A .305 mm PSL is place upon a Si substrate which now has a SiO2 film which is 0.7849 mm thick. We see from the figure that DDFILM follows the scattering measurements very well. No uncertainty bars were included in the data, as the experiment was only conducted once.

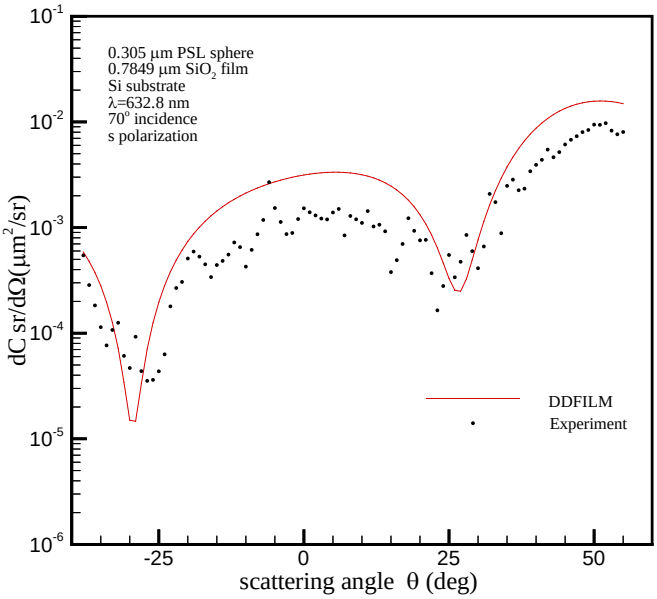

Figure 3.7 $dC_{sca}/d\Omega$ angular variation in the plane of detection for a 0.305 μm PSL sphere on a Si substrate with a 0.25 μm SiO_2 film. Incident beam is at 70 deg incidence, 632.8 nm wavelength, and s polarization.